Pseudo-spectral/finite difference adaptive method for the spherical shallow water equations (SI-CMMSE 2006)

Luis Gavete, Beatriz Alonso, Francisco Ureña, Juan J Benito, Julian Herranz

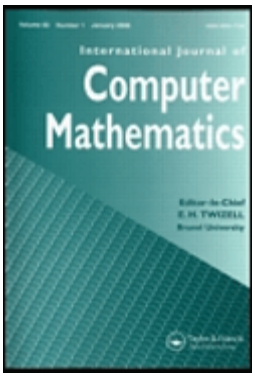

Pseudo-spectral/finite difference adaptive method for the spherical shallow water equations (SI-CMMSE 2006)

Journal:	*International Journal of Computer Mathematics*
Manuscript ID:	GCOM-2006-0160.R1
Manuscript Type:	Original Article
Date Submitted by the Author:	20-Dec-2006
Complete List of Authors:	Gavete, Luis; E.T.S. Ingenieros de Minas, Universidad Politécnica de Madrid, Applied Mathematics in Natural Resources Alonso, Beatriz; E.T.S. Ingenieros de Minas, Universidad Politécnica de Madrid, Applied Mathematics in Natural Resources Ureña, Francisco; Universidad de Castilla La Mancha, Matemática Aplicada Benito, Juan; Universidad Nacional Educación a Distancia, Ingeniería de Construcción y Fabricación Herranz, Julian; E.T.S. Ingenieros de Minas, Universidad Politécnica de Madrid, Applied Mathematics in Natural Resources
Keywords:	shallow water, p-adaptive, finite difference, pseudo-spectral, partial differential equations

A pseudo-spectral/finite difference adaptive method for the spherical shallow water equations (SI-CMMSE 2006)

LUIS GAVETE*§, BEATRIZ ALONSO§, FRANCISCO UREÑA¤, JUAN JOSÉ BENITOЖ AND JULIAN HERRANZ§

§ Department of Applied Mathematics in Natural Resources, Universidad Politécnica de Madrid, Spain
¤Department of Applied Mathematics, Castilla-La Mancha University, Ciudad Real, Spain
ж Department of Construction and Production, UNED, Spain

*Corresponding author. Email: lu.gavete@upm.es

Abstract

The shallow water equations (SWE), describing a thin layer of fluid flow (liquid or gas) in two dimensions, is the simplest possible model that captures the essential characteristics of fluid flow on the sphere. In this paper we present a p-adaptive method based in higher order finite differences and pseudo-spectral derivatives that is applied in the solution of shallow water equations on the sphere. The numerical experiments confirm the expected high-order accuracy.

Keywords: shallow water, p-adaptive, finite difference, pseudo-spectral, partial differential equations

AMS Subject Classification: 65M50, 65M20, 76B60, 86A10

1 Introduction

The shallow water equations (SWE), which describe the flow of a thin layer of fluid in two dimensions have been used by the atmospheric modelling community as a vehicle for testing promising numerical methods for solving atmospheric and oceanic problems. The SWE are important for the study of the dynamics of large-scale flows, as well for the development of new numerical schemes that are applied to more complex models.

There exists a relatively large group of numerical methods for solving the SWE on a sphere, each of them having advantages and disadvantages concerning accuracy, efficiency, reliability, conservation, flexibility, scalability, etc.

One of the most popular class of methods for solving flow problems on the sphere is the spectral transform method (STM) [1,2]. STM expresses the variables as series expansions in terms of the spherical harmonic basis functions, and is known for its high level of accuracy and for being extremely stable. Fornberg [3-5] completed a successful numerical analysis of a simpler set of fluid flow equations on a spherical geometry using a pseudo-spectral method.

An active research area today is the development of numerical methods for solving partial differential equations using adaptively refined grids. Adaptive methods increase the order of accuracy locally, thereby treating to distribute the discretization error uniformly. In this study we present a p-adaptive method for the solution of the shallow water on the sphere. The method combines different approximations (Finite Difference/Pseudo-spectral) of the spatial derivatives using an error indicator. Based on a set of standardized test cases the resulting model performance is investigated.

In section 2, we describe a formulation of the shallow water equations in rectangular coordinates. In section 3 we describe the numerical methods and the p-adaptive scheme used to represent the sphere and to solve the SWE. Williamson et al. [6], proposed a suite of standard tests, for evaluating numerical methods for the SWE in spherical geometry. In section 4 we describe the first two test cases of Williamson and results. For both cases an error analysis is done comparing with Williamson's results and the results of the p-adative scheme are shown. Section 5 contains concluding remarks.

2 The shallow water equations on the sphere

The shallow water equations are a set of equations used to model many fluid flows. They are particularly well suited-and often used-to test numerical techniques for weather prediction. A full formulation of the Shallow Water Equations in spherical coordinates can be found in Holton [7]. The equations are as follows

$$\begin{aligned}
&\frac{\partial h}{\partial t}+\frac{u}{a\cos\theta}\frac{\partial h}{\partial \varphi}+\frac{v}{a}\frac{\partial h}{\partial \theta}+\frac{h}{a\cos\theta}\left[\frac{\partial u}{\partial \varphi}+\frac{\partial\left(v\cos\theta\right)}{\partial \theta}\right]=0\\
&\frac{\partial u}{\partial t}+\frac{u}{a\cos\theta}\frac{\partial u}{\partial \varphi}+\frac{v}{a}\frac{\partial u}{\partial \theta}-\left(f+\frac{u\tan\theta}{a}\right)v+\frac{g}{a\cos\theta}\frac{\partial h}{\partial \varphi}=0 \qquad (1)\\
&\frac{\partial v}{\partial t}+\frac{u}{a\cos\theta}\frac{\partial v}{\partial \varphi}+\frac{v}{a}\frac{\partial v}{\partial \theta}+\left(f+\frac{u\tan\theta}{a}\right)u+\frac{g}{a}\frac{\partial h}{\partial \theta}=0
\end{aligned}$$

where f is the Coriolis parameter, g is the acceleration due to gravity, a is the mean radius of the sphere, h the height function and u and v are the speed of fluid in the φ and θ directions respectively.

We take the globe and map it to a two dimensional grid in (φ,θ) coordinates. The longitude-latitude (φ,θ) grid system used by Fornberg [5] was utilized for computation, with $\varphi\in[-\pi,\pi]$ and $\theta\in\left[-\frac{\pi}{2}+\varepsilon,\frac{\pi}{2}-\varepsilon\right]$. The grid points in this system are arranged so that no grid points are at the poles. This grid system has the advantage of avoiding singularity at the poles and enabling the periodic boundary conditions to be imposed in both longitude and latitude direction. Figure 1 illustrates how the periodic boundary conditions can be imposed in latitude direction.

It should be noted that the sign of the quantities must be adjusted properly when using the periodic boundary condition in latitude direction, depending on whether the quantities are scalar or vector(the velocities change sign as one crosses the pole).

In this study we present a p-adaptive method for the solution of the shallow water on the sphere. Using this adaptive method in the case of solving various coupled partial differential equations, it is possible to employ adaptivity using the standard rectangular grid of Fig. 1 for all the variables involved {h,u,v} in SWE(1). The time integration was done by the fourth-order Runge–Kutta method.

3 P-adaptive scheme

The p-adaptive method is based in higher order finite differences and pseudo spectral derivatives[3](calculated using the fast Fourier transform).

The scheme used to calculate the spatial derivatives are based on three spatial differencing methods: the first one is sixth order accurate, the second one is tenth order accurate and the third one is pseudo-spectral. The type of method used to calculate the derivatives is selected according with an error indicator.

Finite difference methods are attractive because of the relative ease of implementation and flexibility. High order accurate finite difference schemes are important in scientific computation because they offer a means to obtain accurate solutions.

The sixth order finite difference approximation (FD6) of the first derivatives (see Fig. 1) is as follows

$$\left.\frac{\partial f}{\partial \varphi}\right|_{(\varphi_i,\theta_j)} = \left.\frac{\partial f}{\partial \varphi}\right|_{(i,j)} \approx \frac{1}{60\Delta}\left[-f(i-3,j)+9f(i-2,j)-45f(i-1,j)+45f(i+1,j)-9f(i+2,j)+f(i+3,j)\right] \quad (2)$$

$$\left.\frac{\partial f}{\partial \theta}\right|_{(\varphi_i,\theta_j)} = \left.\frac{\partial f}{\partial \theta}\right|_{(i,j)} \approx \frac{1}{60\Delta}\left[-f(i,j-3)+9f(i,j-2)-45f(i,j-1)+45f(i,j+1)-9f(i,j+2)+f(i,j+3)\right]$$

being $\Delta = \frac{\pi}{2M}$.

The tenth order finite difference approximation (FD10) of the first derivatives(see Fig. 1) is as follows

$$\left.\frac{\partial f}{\partial \varphi}\right|_{(\varphi_i,\theta_j)} = \left.\frac{\partial f}{\partial \varphi}\right|_{(i,j)} \approx \frac{1}{2520\Delta}\Big[-2f(i-5,j)+25f(i-4,j)-150f(i-3,j)+600f(i-2,j)-2100f(i-1,j) +2100f(i+1,j)-600f(i+2,j)+150f(i+3,j)-25f(i+4,j)+2f(i+5,j)\Big] \quad (3)$$

$$\left.\frac{\partial f}{\partial \theta}\right|_{(\varphi_i,\theta_j)} = \left.\frac{\partial f}{\partial \theta}\right|_{(i,j)} \approx \frac{1}{2520\Delta}\Big[-2f(i,j-5)+25f(i,j-4)-150f(i,j-3)+600f(i,j-2)-2100f(i,j-1) +2100f(i,j+1)-600f(i,j+2)+150f(i,j+3)-25f(i,j+4)+2f(i,j+5)\Big]$$

Pseudo-spectral techniques are spectrally accurate in space, using all the grid points to calculate the derivatives. Then, the spatial derivatives are calculated more accurately and the spurious oscillations of the solution can be removed. In application of this method, the basic trick is to note that the discrete Fourier transform of an evenly spaced array of N numbers is the wave number for frequency. The discrete Fourier transform(DFT) of an evenly spaced array of N numbers $f_{i,j,}$,that we call f_j in order to simplify the notation for (i=fixed value), is

$$(DFT)_n = \Delta \sum_{j=0}^{N-1} f_j e^{ik_n\theta_j} \quad (4)$$

where Δ is the grid spacing, $k_n = 2\pi \frac{n}{N\Delta}$ is the wave number for frequency n, and θ_j is the position of f_j . The useful part of the discrete Fourier transform is that is invertible by a similar algorithm

$$f_j = \frac{1}{N}\sum_{n=0}^{N-1}(DFT)_n e^{-ik_n\theta_j} \quad (5)$$

Taking the derivative with respect to θ, we get

$$\frac{\partial f_j}{\partial \theta} = \frac{1}{N}\sum_{n=0}^{N-1} -ik_n(DFT)_n e^{-ik_n\theta_j} \quad (6)$$

But that's just the inverse Fourier transform of $-ik_n(DFT)_n$. Therefore the basic pseudo-spectral approach to spatial differencing is to use

$$\frac{\partial f_j}{\partial \theta} = (DFT)^{-1}\left[-ik_n(DFT)\left[f_j\right]\right] \quad (7)$$

and similarly for the φ-first derivative.

Numerically, the pseudo-spectral method involves calls to the fast Fourier transform(FFT). To best utilize FFT's the pseudo-spectral method is confined to 2M points north-south and 4M+1 points east-west where M is a power of two (see Fig. 1). We use the pseudo-spectral method of Fornberg, see Appendix F of [3], that is particularly easy to implement since it is associated with an orthogonal grid (Fig. 1), and all spatial derivatives are obtained by one dimensional approximation along grid lines. After each time step, numerical smoothing (FFT-based) was applied in φ direction (no smoothing was applied in the θ direction).

The p-adaptive scheme used to calculate the spatial derivatives, is completed with the use of an error indicator. Error indicators identify variations and discontinuities within the approximate solution and assume that these are the dominant source of error. For

hyperbolic conservation laws significant errors are generated in both the smooth and discontinuous regions of the flow. The error indicator should have the ability to identify errors in both of the regions. We shall use the indicator of Lönher[8], that we represent here to select the method of approximation of θ-first derivative as

$$\text{ind}_j = \frac{\left|f_{i,j+1} - 2f_{i,j} + f_{i,j-1}\right|}{\left|f_{i,j+1} - f_{i,j}\right| + \left|f_{i,j} - f_{i,j-1}\right| + c} \tag{8}$$

The term c is introduced to filter out small oscillations. The parameter c can be taken to be either a multiple of the local average of $f_{i,j}$ or $c = \beta\left(\left|f_{i,j+1} - f_{i,j}\right| + \left|f_{i,j} - f_{i,j-1}\right|\right)$ for some constant β, or directly a constant c . This indicator is a modified second derivative error norm and has the same characteristics as the normalized 2nd divided difference, but is bounded above by unity. The indicator attempt to identify the location of discontinuities or variations in the smooth flow. For example, in a discontinuity the 2nd divided difference reaches its maximum at the edges of the discontinuity. The constant c is given a value of 0.1. The advantage of this error indicator is that it is dimensionless and entirely local. Then, it can be applied in complete generality to any of the variables of the SWE. By using the values obtained with the error indicator, in order to perform the p-adaptivity we select the type of approximation for the spatial (φ, θ)-derivatives as follows:

$$\left\{\begin{array}{c} \text{ind} \succ 0.01 \Rightarrow \text{Pseudo} - \text{spectral} \\ 0.01 \geq \text{ind} \geq 0.00001 \Rightarrow \text{FD10} \\ \text{ind} \prec 0.00001 \Rightarrow \text{FD6} \end{array}\right\} \tag{9}$$

The same limits for the p-adaptivity have been used for any of the variables of the SWE. Explicit time integration used is based in fourth-order Runge-Kutta(RK4) method.

As it was shown in Fig. 1 the globe is mapped in a two dimensional grid in (φ, θ) coordinates. The p-adaptive process doesn't change the standard rectangular grid of Fig. 1, and uses in all time steps the RK4 method.

According with ref. [3], the stability of the scheme can often be improved by adding some high-order dissipation, a damping of the high frequency modes that does not affect the order of accuracy. Solving SWE on the sphere the convergence of the meridians at the poles demands a short time step in order to satisfy the CFL requirement for computational stability. To avoid severe CFL stability restrictions near the poles after each time step, numerical smoothing (FFT-based) was applied in the φ-direction.

4 Numerical results

Test Cases 1–2 have been used to check the accuracy of the proposed method. The first case in the suite tests the advective component of the numerical method in isolation. Test case 2 (which involves the full set of shallow water equations) has a steady state solution to the non-linear SWE. Detailed mathematical formulas of the test cases and requested performance measurements are described in [6].

4.1 TestCase1: Advection of a Cosine Bell

Test case 1 is a pure advection problem in which a cosine bell is blown around the sphere under a constant velocity field. A cosine bell is advected once around the sphere; the divergence is chosen to be zero for this test case. The cosine bell is discontinuous in the second derivative and this restricts the accuracy of any method which does not specifically compensate for this fact such as an adaptive grid approach.

This test case does not use the full set of the shallow water equations but only the advection equation with a constant velocity field which describes a solid body rotation, so that the height field is transported without any change of shape. The direction of advection can be changed so that the initial data, a compact cosine bell, takes different paths over the computational grid. The earth's rotation is allowed to have an angle α from the coordinate axes to test the capability of the numerical method to handle the pole problem. Thus, by choosing different α's, one can simulate different orientations of the advecting wind, including advection around the equator ($\alpha = 0$), directly over the poles ($\alpha = \pi/2$), and with minor shifts from these two orientations ($\alpha = 0.05$ and $\pi/2-0.05$). The time-step was chosen to be sufficiently small so spatial truncation errors dominate temporal errors, because in this paper we focus on the implementation of a p-adaptive technique for spatial derivatives.

The SWE for this test case is as follows

$$\frac{\partial h}{\partial t}+\frac{u}{a\cos\theta}\frac{\partial h}{\partial \varphi}+\frac{v}{a}\frac{\partial h}{\partial \theta}+\frac{h}{a\cos\theta}\left[\frac{\partial u}{\partial \varphi}+\frac{\partial (v\cos\theta)}{\partial \theta}\right]=0 \qquad (10)$$

the solid body rotation is given by

$$u = u_0(\cos\theta\cos\alpha+\cos(\varphi+\frac{3\pi}{2})\sin\theta\sin\alpha) \qquad (11)$$

$$v = -u_0\sin(\varphi+\frac{3\pi}{2})\sin\alpha \qquad (12)$$

where $u_0 = 2\pi R/(12days)$.

The final difference equation obtained after discretization depends of the values of the error indicator in each time step. For example by using in (10) the sixth order finite difference approximation for the derivatives we have

$$\frac{\partial h_{i,j}}{\partial t}+\frac{u_{i,j}}{a\cos\theta_{i,j}}\frac{1}{60\Delta}\left[\begin{array}{l}-h(i-3,j)+9h(i-2,j)-45h(i-1,j)+\\45h(i+1,j)-9h(i+2,j)+h(i+3,j)\end{array}\right]+$$

$$\frac{v_{i,j}}{a}\frac{1}{60\Delta}\left[\begin{array}{l}-h(i,j-3)+9h(i,j-2)-45h(i,j-1)+\\45h(i,j+1)-9h(i,j+2)+h(i,j+3)\end{array}\right]+ \qquad (13)$$

$$\frac{h_{i,j}}{a\cos\theta_{i,j}}\left[\left.\frac{\partial u}{\partial\varphi}\right|_{(i,j)}+\cos\theta_{i,j}\left.\frac{\partial v}{\partial\theta}\right|_{(i,j)}-v_{i,j}sen\theta_{i,j}\right]=0$$

The algorithm for the Test Case1 is summarized below:

1.-Define input data:

number of grid points
angle between the axis of solid body rotation and the polar axis
h(i,j), u(i,j) and v(i,j) initial data
time step (k)
number of time steps

2.- For each time step

* For each point (i,j):

- Fourth order Runge-Kutta method: $h_{i,j}^{n+1}=h_{i,j}^{n}+\frac{1}{6}(d_1+2d_2+2d_3+d_4)$

$$d_1=k*f\left(t^n,h_{i,j}^n\right)$$

$$d_2=k*f\left(t^n+\frac{k}{2},h_{i,j}^n+\frac{1}{2}d_1\right)$$

$$d_3=k*f\left(t^n+\frac{k}{2},h_{i,j}^n+\frac{1}{2}d_2\right)$$

$$d_4=k*f\left(t^n+k,h_{i,j}^n+d_3\right)$$

$$f(t^n,h_{i,j}^n)=\frac{\partial h_{i,j}}{\partial t}=-\frac{u_{i,j}}{a\cos\theta_{i,j}}\left.\frac{\partial h}{\partial\varphi}\right|_{(i,j)}-\frac{v_{i,j}}{a}\left.\frac{\partial h}{\partial\theta}\right|_{(i,j)}-\frac{h_{i,j}}{a\cos\theta_{i,j}}\left[\left.\frac{\partial u}{\partial\varphi}\right|_{(i,j)}+\left.\frac{\partial(v\cos\theta)}{\partial\theta}\right|_{(i,j)}\right]$$

- Use error indicator to select the approximation of derivatives

* Numerical smoothing (FFT-based) in φ direction

* Error norms calculation

Figure 2 shows the geopotential field h (Cosine bell) after one revolution with the p-adaptive method for $\alpha = 0$. The numerical solution translated in all cases without change of shape.

For the last time step shown in Figure 2, by using the error indicator (4) the p-adaptive results are shown in Fig. 3. Red points (black point in black-and-white print edition) have been calculated with pseudo-spectral derivatives, white points have been calculated with FD10 and blue points (the smallest size points) with FD6.

The errors allow to evaluate the advective properties of the scheme. Errors which are defined in the usual way[6]. The global relative errors on the advected field have been measured in different norms in Fig 4 . We recall here their definition for a generic variable Z:

$$L_1 = \frac{\sum_i \left| Z_i - Z_i^{true} \right|}{\sum_i \left| Z_i^{true} \right|} ; L_2 = \left(\frac{\sum_i \left(Z_i - Z_i^{true} \right)^2}{\sum_i \left(Z_i^{true} \right)^2} \right)^{1/2} ; L_\infty = \max_i \frac{\left| Z_i - Z_i^{true} \right|}{\left| Z_i^{true} \right|} \qquad (14)$$

It is interesting to compare the p-adaptive method with a numerical standard technique, for example, using FD6 in all the points of the unrolled sphere. Then in Fig. 5, the L_2 –error obtained with the p-adaptive method is compared with the error obtained in the case of using the FD6 approximation in all the points.

4.2 Test CASE 2: Global Steady State Nonlinear Zonal Geostrophic Flow

To test the p-adaptive scheme on the full SWE, we used Test case 2 in [6], Global Steady State Nonlinear Zonal Geostrophic Flow, which has a steady state solution to the non-linear SWE (1). In this test initially $h(\varphi,\theta)$ is described by

$$gh(\varphi,\theta) = gh_0 - \left(a\Omega u_0 + \frac{u_0^2}{2}\right)\left(-\cos\varphi\cos\theta\sin\alpha + \sin\theta\cos\alpha\right)^2 \qquad (15)$$

where $gh_0 = 2.94x10^4\, m^2/s^2$, g is the gravitational constant and u_0 and α, as they were in test case 1. For this case 2, the test pattern should retain the same shape on the sphere for {h,u,v} throughout all the rotation. The solution is stationary in time.

The final difference equation obtained after discretization depends of the values of the error indicator in each time step. For example by using in (1) the tenth order finite difference approximation for the {h, u, v}-derivatives we have

$$
\begin{aligned}
&\frac{\partial h_{i,j}}{\partial t}+\frac{u_{i,j}}{a\cos\theta_{i,j}}\frac{1}{2520\Delta}\begin{bmatrix}-2h(i-5,j)+25h(i-4,j)-150h(i-3,j)+600h(i-2,j)\\-2100h(i-1,j)+2100h(i+1,j)-600h(i+2,j)+\\150h(i+3,j)-25h(i+4,j)+2h(i+5,j)\end{bmatrix}\\
&+\frac{v_{i,j}}{a}\frac{1}{2520\Delta}\begin{bmatrix}-2h(i,j-5)+25h(i,j-4)-150h(i,j-3)+600h(i,j-2)-2100h(i,j-1)\\+2100h(i,j+1)-600h(i,j+2)+150h(i,j+3)-25h(i,j+4)+2h(i,j+5)\end{bmatrix}\\
&+\frac{h_{i,j}}{a\cos\theta_{i,j}}\frac{1}{2520\Delta}\begin{bmatrix}-2u(i-5,j)+25u(i-4,j)-150u(i-3,j)+600u(i-2,j)\\-2100u(i-1,j)+2100u(i+1,j)-600u(i+2,j)+\\150u(i+3,j)-25u(i+4,j)+2u(i+5,j)\end{bmatrix}\\
&+\frac{h_{i,j}}{a}\frac{1}{2520\Delta}\begin{bmatrix}-2v(i,j-5)+25v(i,j-4)-150v(i,j-3)\\+600v(i,j-2)-2100v(i,j-1)+2100v(i,j+1)\\-600v(i,j+2)+150v(i,j+3)-25v(i,j+4)+2v(i,j+5)\end{bmatrix}\\
&-\frac{h_{i,j}}{a\cos\theta_{i,j}}v_{i,j}sen\theta_{i,j}=0\\
&\frac{\partial u_{i,j}}{\partial t}+\frac{u_{i,j}}{a\cos\theta_{i,j}}\frac{1}{2520\Delta}\begin{bmatrix}-2u(i-5,j)+25u(i-4,j)-150u(i-3,j)+600u(i-2,j)\\-2100u(i-1,j)+2100u(i+1,j)-600u(i+2,j)+\\150u(i+3,j)-25u(i+4,j)+2u(i+5,j)\end{bmatrix}\\
&+\frac{v_{i,j}}{a}\frac{1}{2520\Delta}\begin{bmatrix}-2u(i,j-5)+25u(i,j-4)-150u(i,j-3)\\+600u(i,j-2)-2100u(i,j-1)+2100u(i,j+1)\\-600u(i,j+2)+150u(i,j+3)-25u(i,j+4)+2u(i,j+5)\end{bmatrix}\\
&-\left(f_{i,j}+\frac{u_{i,j}\tan\theta_{i,j}}{a}\right)v_{i,j}\\
&+\frac{g}{a\cos\theta_{i,j}}\frac{1}{2520\Delta}\begin{bmatrix}-2h(i-5,j)+25h(i-4,j)-150h(i-3,j)+600h(i-2,j)\\-2100h(i-1,j)+2100h(i+1,j)-600h(i+2,j)\\+150h(i+3,j)-25h(i+4,j)+2h(i+5,j)\end{bmatrix}=0\\
&\frac{\partial v_{i,j}}{\partial t}+\frac{u_{i,j}}{a\cos\theta_{i,j}}\frac{1}{2520\Delta}\begin{bmatrix}-2v(i-5,j)+25v(i-4,j)-150v(i-3,j)+600v(i-2,j)\\-2100v(i-1,j)+2100v(i+1,j)-600v(i+2,j)\\+150v(i+3,j)-25v(i+4,j)+2v(i+5,j)\end{bmatrix}\\
&+\frac{v_{i,j}}{a}\frac{1}{2520\Delta}\begin{bmatrix}-2v(i,j-5)+25v(i,j-4)-150v(i,j-3)\\+600v(i,j-2)-2100v(i,j-1)+2100v(i,j+1)\\-600v(i,j+2)+150v(i,j+3)-25v(i,j+4)+2v(i,j+5)\end{bmatrix}\\
&+\left(f_{i,j}+\frac{u_{i,j}\tan\theta_{i,j}}{a}\right)u_{i,j}\\
&+\frac{g}{a}\frac{1}{2520\Delta}\begin{bmatrix}-2h(i,j-5)+25h(i,j-4)-150h(i,j-3)+600h(i,j-2)\\-2100h(i,j-1)+2100h(i,j+1)-600h(i,j+2)\\+150h(i,j+3)-25h(i,j+4)+2h(i,j+5)\end{bmatrix}=0
\end{aligned}
\tag{16}
$$

The algorithm used for TestCase2 is similar to the one of Test case 1, but RK4 is applied to the system of differential equations(16), to obtain h, u and v for each time step.

Figure 6 gives the results obtained for h(geopotential field),u(velocity),v(velocity) after one revolution for with the p-adaptive method for $\alpha = \frac{\pi}{2} - 0.05$ with M=16. Also in Figure 6, by using the error indicator (4) the p-adaptive results are shown. As it is shown the accuracy of the approximation of the derivatives is different for {h,u,v} depending of the error indicator obtained for each one of the variables. Red points (black point in black-and-white print edition) have been calculated with pseudo-spectral derivatives, white points have been calculated with FD10 and blue points (the smallest size points) with FD6. In this case we have solved the full set of SWE and the p-adaptive method can give in each point (φ, θ) a different p-approximation for the {h, u, v}-derivatives using the standard grid of Fig.1.

Figure 7 shows the norm errors in the geopotential field after one revolution with the p-adaptive method for $\alpha = \frac{\pi}{2} - 0.05$ with M=16. We observe that the p-adaptive scheme is numerically very stable.

It is interesting to compare the p-adaptive method with a numerical standard technique, for example using FD6 in all the points of the unrolled sphere. Then in Fig. 8 the L_2 –error obtained with the p-adaptive method is compared with the error obtained in the case of using the FD6 approximation in all the points.

5 Conclusions

A p-adaptive method for solving the SWE on the sphere based on a regular latitude-longitude grid, has been developed and tested. The method combines different approximations (Finite Difference/Pseudo-spectral) of the spatial derivatives using an error indicator. Explicit time integration used is based in fourth-order Runge-Kutta method.

Figures presented in this work have shown the ability of the p-adaptive method to treat the presence of strong gradients. The ability of the p-adaptive method is increased in the case of solving the full SWE. Then, the p-adaptivity is applied at the same time in the three variables of equations (1) using the regular latitude-longitude grid.

The p-adaptive method is computationally efficient. Validation of the algorithm has been carried out using the standard test set of Williamson. Application to the standard test set (cases one and two) for the shallow water equations shows the high accuracy and flexibility of the p-adaptive scheme.

The test results presented in this study show that our method is thought to be promising for a variety of numerical models including p-adaptive high-resolution models for weather prediction. Computational results demonstrating the accuracy have been presented.

Acknowledgement

The authors acknowledge the support from Ministerio de Educación y Ciencia of Spain, project CGL2004-04095/CLI, and the support from Consejería de Educación y Ciencia de la Junta de Comunidades de Castilla-la Mancha of Spain, project PA106-0123-7821.

References

[1] P. N. SWARZTRAUBER, "Spectral transform methods for solving the shallow water equations on the sphere". *Monthly Weather Review* **124** (2000) 730–744.

[2] M. TAYLOR, J. TRIBBIA, and M. ISKANDARANI. "The spectral element method for the shallow water equations on the sphere", *Journal of Computational Physics* **130,1**(1997) 92–108.

[3] B. FORNBERG, *A Practical Guide to Pseudospectral Methods*, Cambridge University Press, 1996.

[4] B. FORNBERG, "A Pseudospectral Approach for Polar and Spherical Geometries", *SIAM Journal of Scientific Computing*, **16, 5**, (1995) 1071-1081.

[5] B. FORNBERG, D. MERRILL, "Comparison of finite difference and pseudospectral methods for convective flow over a sphere", *Geophysic Res. Lett.*,**24**, (1997), 3245-3248.

[6] D. L. WILLIAMSON, J. B. DRAKE, J. J. HACK, R. JAKOB, and P. N. SWARZTRAUBER, "A Standard Test Set for Numerical Approximations to the Shallow Water Equations in Spherical Geometry", *Journal of Computational Physics*, **102(1)**, (1991) 211–224.

[7] J. R. HOLTON, *An Introduction to Dynamic Meteorology*, Academic Press, New York, London, 1972.

[8] H. LUO, J.D. BAUM, and R. LÖHNER, "An efficient spatial adaption algorithm on 3-d unstructured meshes for the euler equations", 1993.

List of figure captions

Figure 1: Unrolling the sphere onto a two dimensional grid.

Figure 2: Cosine bell after one revolution with the p-adaptive method for $\alpha = 0$ with M=16.

Figure 3: P-adaptivity in the geopotential field after one revolution for $\alpha = 0$ with M=16

Figure 4: Errors in the geopotential field after one revolution with the p-adaptive method for $\alpha = 0$ with M=16

Figure 5: L2 norm with p-adaptive method and FD6 in CaseTest1 for $\alpha = 0$ with M=16

Figure. 6: h(geopotential field), u(velocity) and v(velocity) after one revolution with the p-adaptive method for $\alpha = \frac{\pi}{2} - 0.05$ and M=16.

Figure 7 : **N**orm errors in the geopotential field after one revolution with the p-adaptive method for $\alpha = \frac{\pi}{2} - 0.05$ with M=16.

Figure 8: L2 norm with p-adaptive method and FD6 in CaseTest2 for $\alpha = \frac{\pi}{2} - 0.05$ with M=16

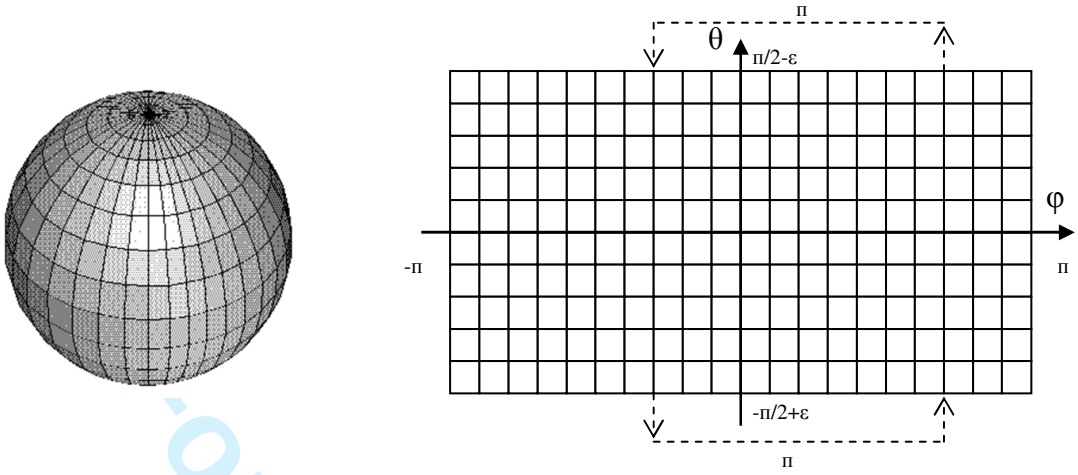

Figure 1: Unrolling the sphere onto a two dimensional grid.

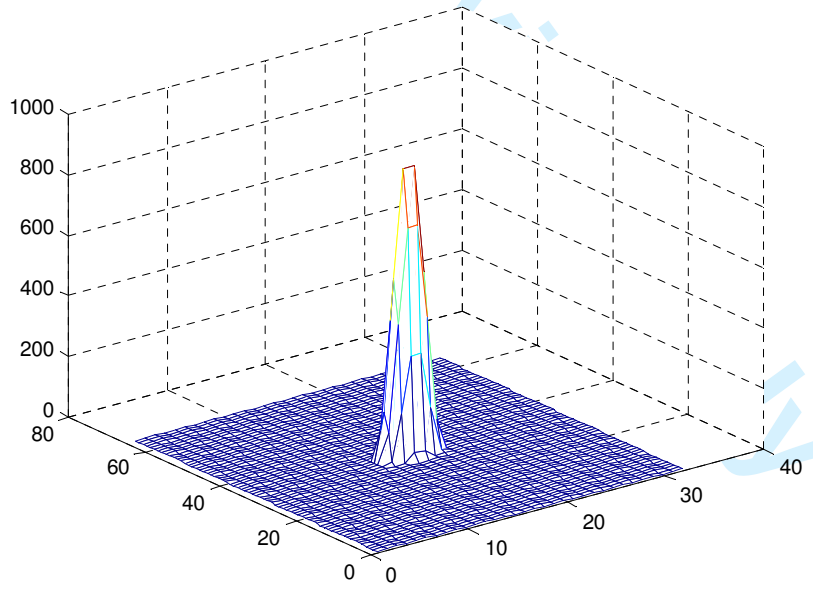

Figure 2: Cosine bell after one revolution with the p-adaptive method for $\alpha = 0$ with M=16.

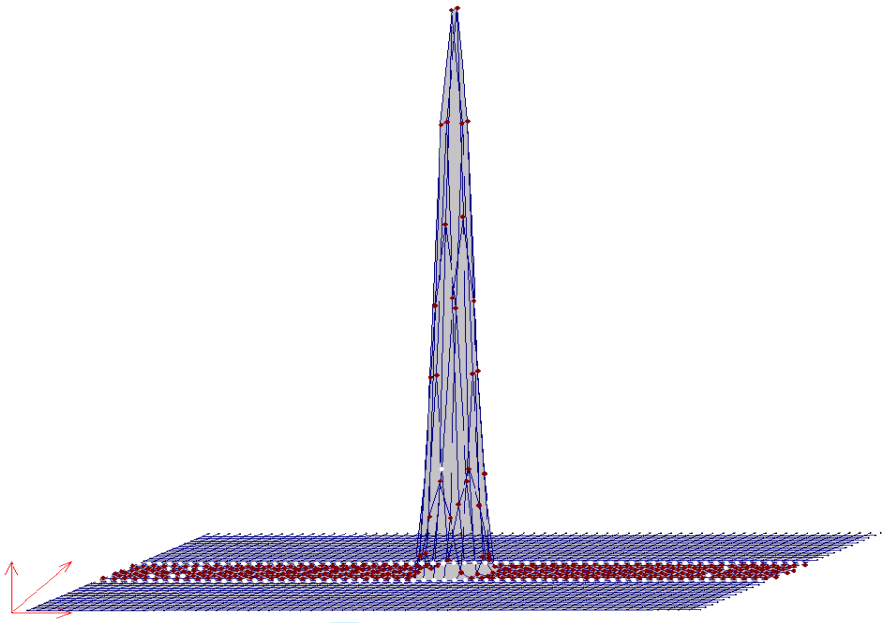

Figure 3: P-adaptivity in the geopotential field after one revolution for $\alpha = 0$ with M=16

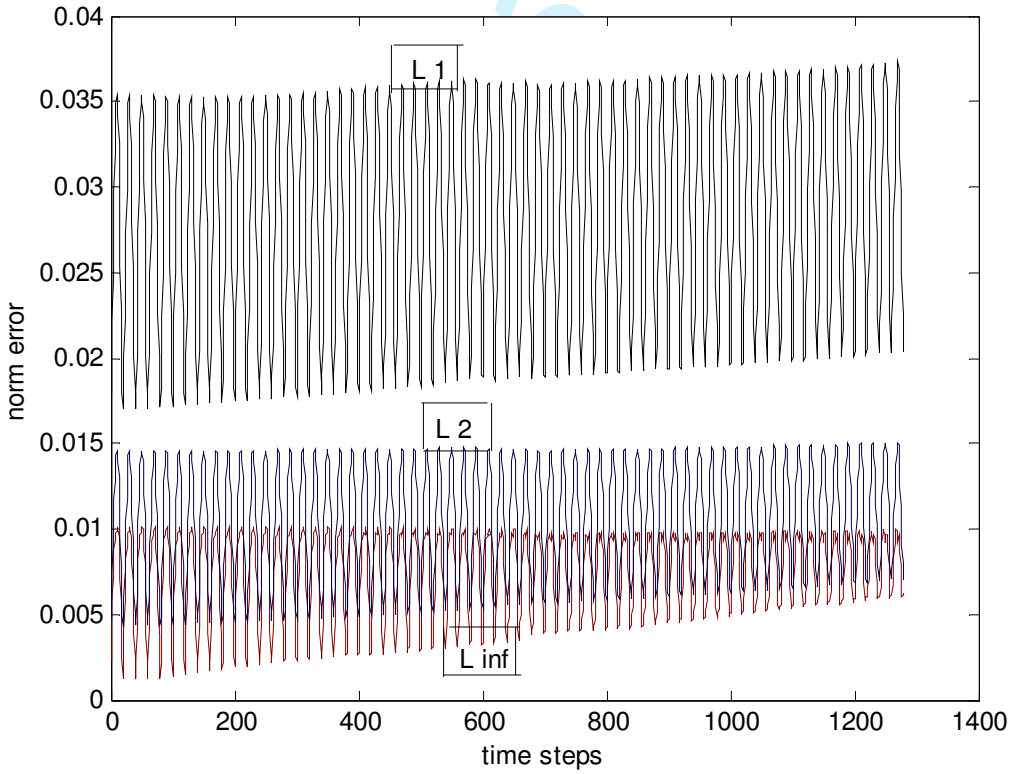

Figure 4: Errors in the geopotential field after one revolution with the p-adaptive method for $\alpha = 0$ with M=16

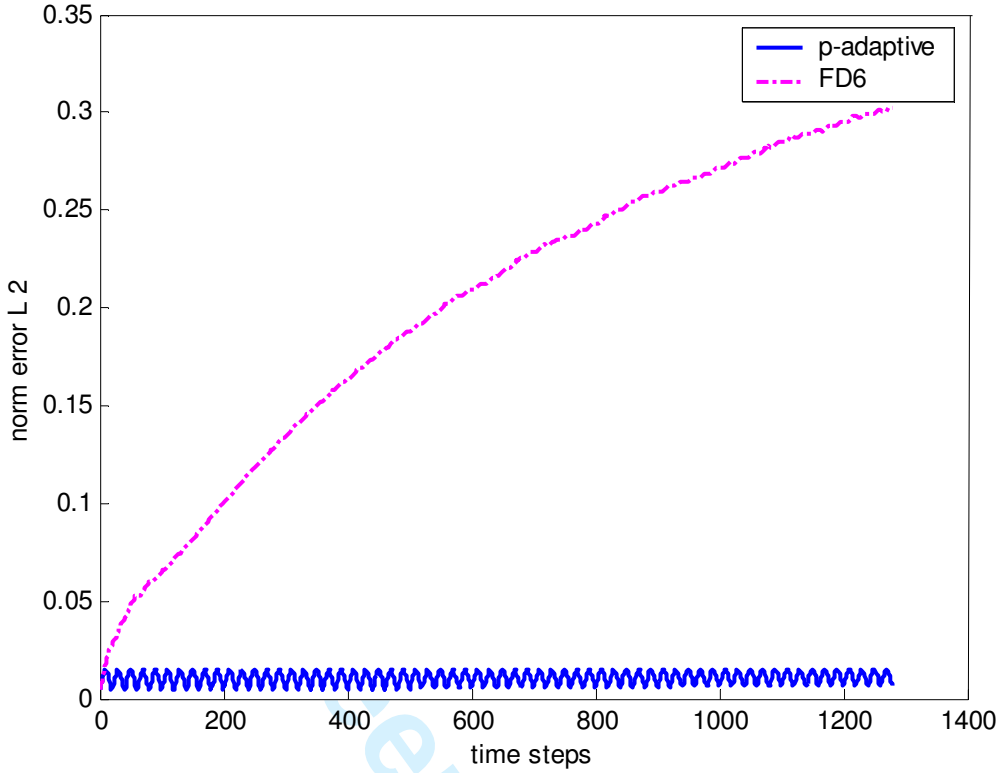

Figure 5. L2 norm with p-adaptive method and FD6 in CaseTest1 for $\alpha = 0$ with M=16

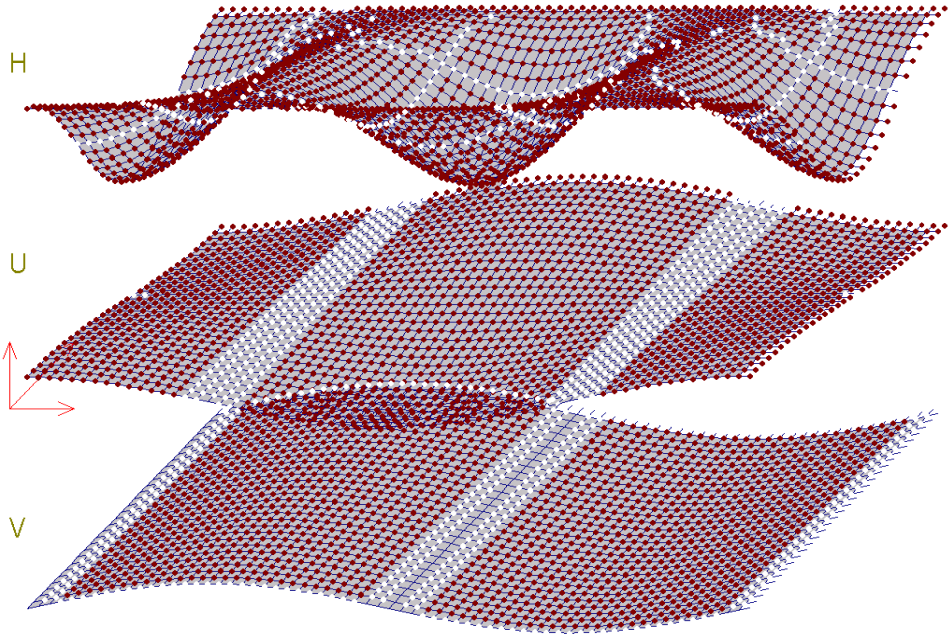

Figure. 6: h(geopotential field), u(velocity) and v(velocity) after one revolution with the p-adaptive method for $\alpha = \frac{\pi}{2} - 0.05$ and M=16.

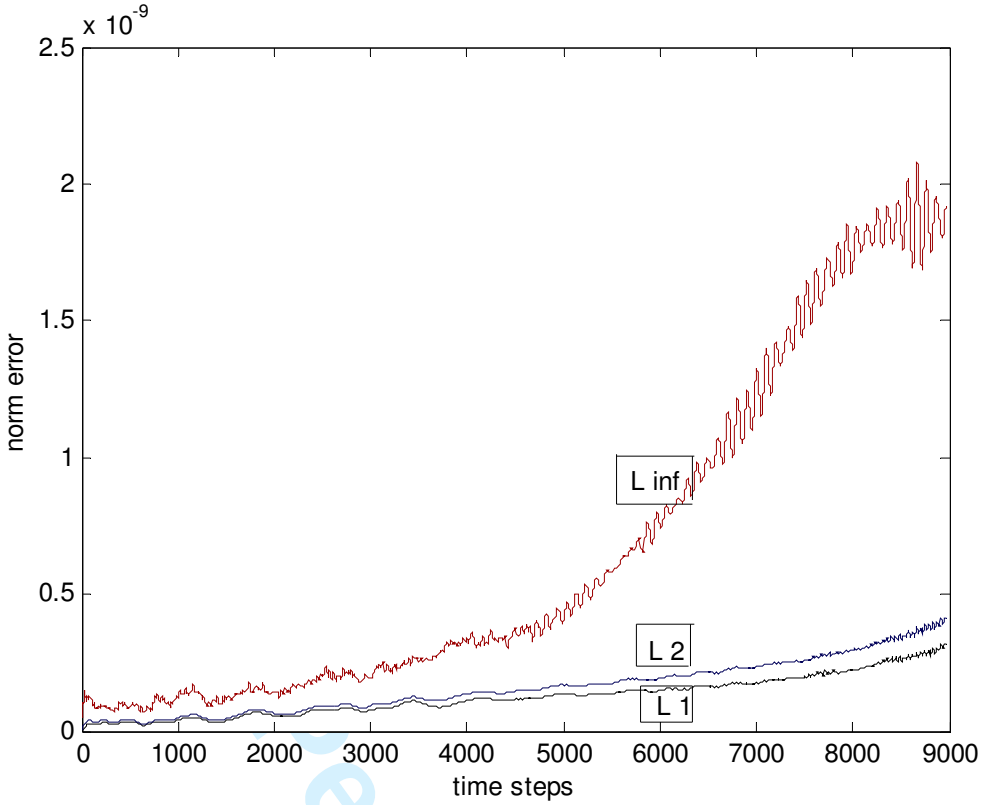

Figure 7 : Norm errors in the geopotential field after one revolution with the p-adaptive method for $\alpha = \frac{\pi}{2} - 0.05$ with M=16.

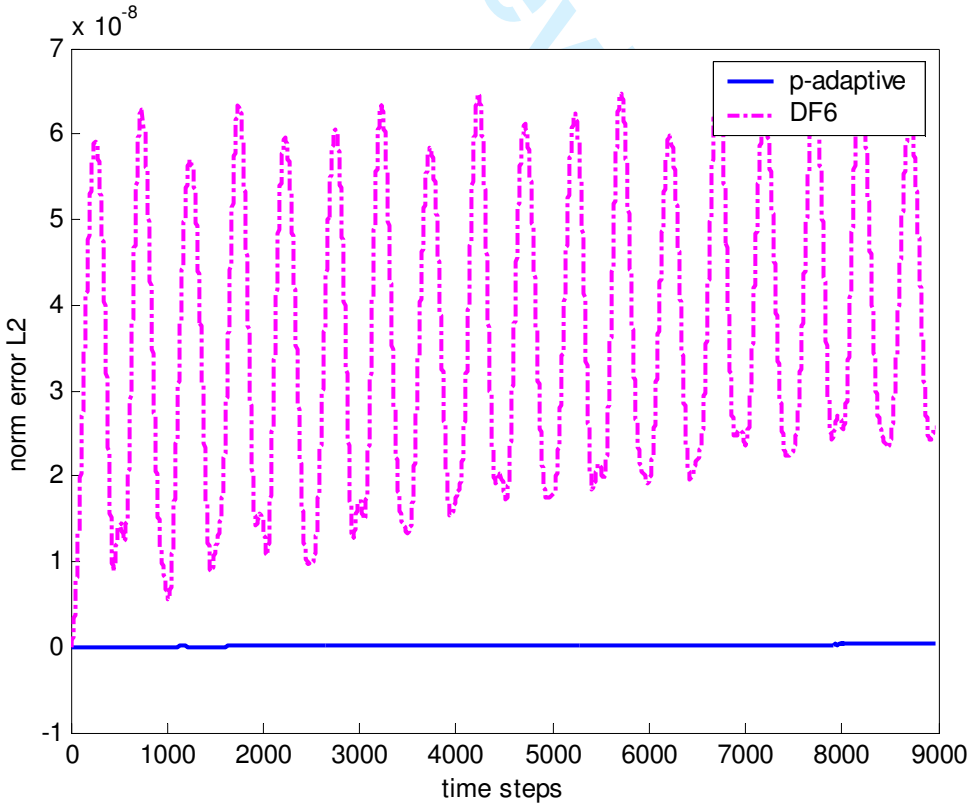

Figure 8. L2 norm with p-adaptive method and FD6 in CaseTest2 for $\alpha = \frac{\pi}{2} - 0.05$ with M=16.

List of figure captions

Figure 1: Unrolling the sphere onto a two dimensional grid.

Figure 2: Cosine bell after one revolution with the p-adaptive method for $\alpha = 0$ with M=16.

Figure 3: P-adaptivity in the geopotential field after one revolution for $\alpha = 0$ with M=16

Figure 4: Errors in the geopotential field after one revolution with the p-adaptive method for $\alpha = 0$ with M=16

Figure 5: L2 norm with p-adaptive method and FD6 in CaseTest1 for $\alpha = 0$ with M=16

Figure. 6: h(geopotential field), u(velocity) and v(velocity) after one revolution with the p-adaptive method for $\alpha = \frac{\pi}{2} - 0.05$ and M=16.

Figure 7 : Norm errors in the geopotential field after one revolution with the p-adaptive method for $\alpha = \frac{\pi}{2} - 0.05$ with M=16.

Figure 8: L2 norm with p-adaptive method and FD6 in CaseTest2 for $\alpha = \frac{\pi}{2} - 0.05$ with M=16